Applied Geochemistry 170 (2024) 106087

Contents lists available at ScienceDirect

Applied Geochemistry

journal homepage: www.elsevier.com/locate/apgeochem

Uptake of Cm (III) and Eu (III) by C–S–H phases under saline conditions in presence of EDTA: A batch sorption and TRLFS study

Aline K. Thumm *, Andrej Skerencak-Frech, Xavier Gaona, Marcus Altmaier, Horst Geckeis

Institute for Nuclear Waste Disposal, Karlsruhe Institute of Technology, P.O. Box 3640, 76201, Karlsruhe, Germany

ARTICLE INFO

Editorial Handling by: Barbara Lothenbach

Keywords:
C-S-H phases
EDTA
Sorption
Radionuclides
Eu(III)
Cm(III)
TRLFS
Saline conditions
NaCl
$CaCl_2$
Adsorption
Kinetics

ABSTRACT

Eu (III) and Cm (III) uptake by calcium silicate hydrate phases (C–S–H) was investigated in presence of EDTA in NaCl and $CaCl_2$ solutions. Different experimental parameters, *i.e.,* ionic strength (0.1 m $\leq I_m \leq$ 5.05 m), ligand concentration (10^{-5} m $\leq$ [EDTA] $\leq 10^{-2}$ m), calcium-to-silicon ratio (0.6 $\leq$ C/S $\leq$ 1.3) and sorption time (7 d $\leq t \leq$ 365 d) were varied in the frame of batch sorption experiments and Time Resolved Laser Fluorescence spectroscopy (TRLFS) measurements. No effect of EDTA on the retention of Eu(III)/Cm(III) by C–S–H phases in NaCl or $CaCl_2$ systems was observed at ligand concentrations $\leq 10^{-3}$ M. In NaCl solutions with [EDTA] = 10^{-2} M and C/S < 1.3, low retention (log R_d = 2–3, with R_d in L•kg^{-1}) of Eu(III) was detected after 7 d of sorption time, while strong retention (log R_d = 5–6) was observed after 50 d. This behaviour was explained by the initial stabilization of Eu(III)/Cm(III) in the aqueous phase due to the formation of two aqueous Eu(III)/Cm(III)-$(OH)_n$-EDTA complexes, followed by the slow incorporation of Eu(III)/Cm(III) into the C–S–H structure. In $CaCl_2$ solutions for all C/S ratios, as well as in NaCl solutions for C/S ~ 1.3, the presence of [EDTA] = 10^{-2} M led to a significant decrease of the uptake (log R_d = 2–3) after 7 and 50 d of contact time. This effect was explained by the formation of stable aqueous Ca–Eu(III)/Cm(III)-EDTA complexes triggered by the presence of moderate to high Ca concentrations. No evident effect caused by increased ionic strength conditions could be confirmed in our sorption experiments.

Results obtained in batch sorption experiments are underpinned by TRLFS data, with the observation of three main aqueous species, tentatively defined as Cm(OH)(EDTA)$^{2-}$, Cm$(OH)_x$ (EDTA)$^{-(x+1)}$ and Ca–Cm(III)-EDTA, as well as a fourth species corresponding to Cm(III) incorporated in the CaO-layer of the C–S–H phases. In spite of the thermodynamic stability of the CaEDTA^{2-} complex, which reduces the concentration of free EDTA, the formation of ternary Ca–Eu(III)/Cm(III)-EDTA complexes is expected to result in a significant impact of EDTA on the uptake of *An* (III)/Ln (III) by cement at high ligand concentrations. The assumption that Ca outcompetes actinides for the complexation with EDTA in cementitious systems may need to be revisited under these conditions.

1. Introduction

Storage of radioactive waste in deep geological formations represents the preferred option for its disposal in Germany as well as in other countries. The disposal concept will consist of a multibarrier system, including different technical, geo-technical and geological barriers. Minimizing the release of radionuclides (RN) into the geo- and biosphere is the primary objective. The intrusion of water may result in the formation of aqueous systems, possibly leading to the mobilization of RN into the geosphere. Besides solubility phenomena, sorption processes to mineral phases are the primary reactions leading to an effective retardation of RNs. The accurate description of RN migration requires a comprehensive quantification of these processes, as well as a detailed understanding of the sorption mechanism of the most relevant RN with the mineral phases present in the near- and far field of a repository on the molecular scale (Bube et al., 2013). Radioactive waste is typically classified into three main categories based on its level of radioactivity and associated heat generation: (i) High Level Radioactive Waste (HLW)/High Active Radioactive Waste (HAW), (ii) Intermediate Level Radioactive Waste (ILW), and (iii) Low Level Radioactive Waste (LLW) (Lersow and Waggitt 2020). HLW or HAW is characterized by its significant heat generation, which is attributed to spent fuel elements and

* Corresponding author.
E-mail address: aline.thumm@kit.edu (A.K. Thumm).

https://doi.org/10.1016/j.apgeochem.2024.106087
Received 25 March 2024; Received in revised form 17 June 2024; Accepted 27 June 2024
Available online 28 June 2024

vitrified waste from reprocessing. ILW and LLW describe waste with comparatively low RN content and thus with low or negligible heat generation. The two latter waste forms constitute the largest volume fraction of radioactive waste in Germany (Rübel et al., 2004). ILW and LLW originate from diverse sources, including the dismantling of nuclear facilities, industrial processes, research and development activities and medical applications of radioactive materials (Osterhage and Frey 2022). Hence, the waste mixture of L/ILW is highly heterogenous, with a large variety of different RN as well as inorganic and organic compounds.

L/ILW is usually conditioned by mixing with and embedding in cementitious matrices (Tits et al., 2006, Ochs et al., 2016). Concrete is also used for construction purposes of a waste repository. C–S–H phases are the main binding component of cementitious materials and offer high specific surface areas, leading to high sorption capacities for tri- and tetravalent actinides (*An* (III)/*An* (IV)) (Pointeau et al., 2001; Li and Pang 2014; Tits et al., 2006). Aqueous solutions in contact with cemented radioactive waste are characterized by high pH values in the alkaline to hyperalkaline region (pH = 9–13.3) (Bube et al., 2013; Wieland 2014; Tits and Wieland 2018). Strongly reducing conditions evolve during corrosion of steel barrels, in which the cemented waste is filled in, so that *An* predominantly exist in their tri- and tetravalent oxidation state.

Organic L/ILW waste components comprise strongly complexing agents including EDTA (ethylenediaminetetraacetic acid), due to its application as decontamination agent in nuclear facilities (Colàs et al., 2013; Hummel et al., 2005). EDTA provides four carboxylic acid functional groups as well as two free electron lone pairs on the two nitrogen atoms, leading to a hexadentate chelating ligand with strong complexing properties towards tri- or tetravalent metal ions in aqueous media (Holleman 2019; Keith-Roach 2008). The formation of stable *An* (III)/*An* (IV)-EDTA complexes in the aqueous phase may increase the mobility of the actinides due to the increase of their solubility as well as the suppression of sorptions reactions with mineral phases.

In the past decades, the uptake of Eu(III)/Cm(III) on C–S–H phases was mostly studied in absence of organic ligands and at low ionic strength conditions ($I_m \leq 0.1$ m). Pointeau et al. conducted batch sorption experiments to examine the sorption of Eu(III) on C–S–H phases (Pointeau et al., 2001). They revealed rapid sorption of Eu(III) and an exceptionally high, nearly quantitative retention on C–S–H phases (~98 %). Tits et al. studied the Eu(III) uptake on C–S–H phases in the frame of batch sorption experiments and obtained a very high retention of Eu(III) with log $R_d \sim 6$ (R_d in L•kg^{-1}) (Tits and Wieland 2018). Moreover, Tits *et al.* investigated the sorption of Cm(III) on C–S–H phases with TRLFS (Tits et al., 2003). They observed, that the strong retention of Cm(III) is due to an incorporation into the C–S–H phase by exchanging Ca^{2+} from the CaO interlayer. In addition, the uptake of Cm(III) by the hardened cement paste (HCP) was investigated by Stumpf *et al.*, also confirming an incorporation of Cm(III) into the interlayer of the C–S–H phases of the HCP (Stumpf et al., 2004). Generally, the interaction process between Eu (III)/Cm(III) and C–S–H phases is presumed to follow a two-step process, whereas the trivalent metal ion forms surface complexes, which is followed by a slower incorporation of the metal ion into the C–S–H phase (Tits and Wieland 2018; Pointeau et al., 2001; Schlegel et al., 2004; Macé et al., 2013; Tits et al., 2003; Mandaliev et al., 2011).

Literature data concerning the Eu(III) and Cm(III) uptake on C–S–H phases and cementitious materials in presence of organics are limited. The sorption of Eu(III) on C–S–H phases in the presence of Gluconate (GLU) was investigated by Wieland *et al.*: The retention of Eu(III) decreased significantly at [GLU] $\geq 10^{-4}$ M (Wieland 2014). Guidone et al. also studied the retention of Eu(III) on C–S–H phases in presence of GLU and obtained similar results (Guidone 2023). These observations were explained by the formation of aqueous ternary Ca–Eu(III)-GLU complexes. Similar observations were reported by Tasi *et al.*, who studied the Cement-Pu(IV)-ISA system. The authors observed a decrease of log R_d values of Pu at $[Pu]_{tot} = 1 \cdot 10^{-9}$ M at [ISA] $\geq 10^{-4}$ M, which was explained by the formation of ternary Ca–Pu(IV)-ISA and quaternary Ca–Pu(IV)–OH-ISA aqueous complexes (Tasi et al. 2018, 2021). However, at high ligand concentrations, they observed an increase in the uptake, which was attributed to the formation of surface complexes involving Pu(IV) and ISA.

EDTA has been usually considered to have a negligible impact on the retention or RN in cementitious environments due to the strong complexation with Ca, being present at concentration levels higher than RN by orders of magnitude and, thus, outcompeting the possible complexation of the ligand with RN. Maragkou *et al.* studied the sorption of EDTA on C–S–H phases. The authors concluded, that destabilization of the C–S–H phase is observed at [EDTA] > 0.01 M. However, these effect were not further described in detail (Maragkou and Pashalidis 2021). For [EDTA] < 0.01 M, the results indicated a sorption of the organic ligand on the C–S–H phase through *e.g.* Ca-EDTA surface complexes. Therefore, it is the concentration of EDTA that is the key factor in their study.

Drtinova *et al.* studied Eu(III) sorption on C–S–H phases (C/S = 1.0) in the presence of EDTA ([EDTA] = 5•10^{-5} - 5•10^{-3} M). They concluded that at ligand concentrations $\leq 5 \bullet 10^{-3}$ M, EDTA does not impact the uptake of Eu(III) by C–S–H phases. Ochs *et al.* conducted a comparative evaluation using experimental data and thermodynamic calculations for the assessment of ISA/EDTA-actinide-cement systems (Ochs et al., 2022). Based on previous data reported by Dario and co-workers (Dario et al., 2004), Ochs *et al.* concluded that the effect of EDTA on the retention of Eu(III) is negligible at [EDTA] < 0.1 M (Ochs et al., 2022). A detailed inspection of the original source reveals a shift by a factor of 1000 in these Figures, *i.e.*, R_d values for the uptake of Eu(III) ($[Eu(III)]_{tot} = 1 \cdot 10^{-8}$ M) by cement decrease at [EDTA] > 10^{-4} M. Pointeau et al. investigated also the uptake of EDTA by fresh (pH = 13.3) and degraded (pH = 11.9) cement, and reported $R_d \approx 0.1$ and 10 L kg^{-1}, respectively. This behaviour was explained with the evolution of the calcium concentration in the pore water and surface potential/charge of the hydrated cement (Pointeau et al., 2006). A more comprehensive study on the sorption of organic ligands to cementitious materials is provided by Szabo *et al.*: They reported, that EDTA with four –COOH and two amine groups shows similar R_d values as glutaric acid with only two –COOH groups. It appears that only a limited number of carboxylate entities in organic ligands interact with cementitious material and steric constraints have to be considered (Szabo et al., 2022).

The focus of this work is on the impact of EDTA on the uptake of Eu (III) and Cm(III) on C–S–H phases. Diluted to concentrated NaCl and $CaCl_2$ solutions (I_m = 0.1–5.36 m) were used. Aqueous solutions of higher ionic strengths are of relevance in host rock formations in the vicinity of rock salt layers. Such conditions are given *e.g.* in northern German clay rock formations (Brewitz 1982). The uptake of Eu(III) was quantified by classical batch sorption experiments, while the species in the aqueous and solid phase were identified by TRLFS with Cm(III).

2. Materials and methods

2.1. Materials

The experimental procedures were carried out under inert gas conditions within an argon-filled glovebox ($O_2 \sim 2$ ppm, 99% Ar), to ensure the exclusion of CO_2.

In all experiments, the ionic strength was adjusted using NaCl (*Honeywell Specialty Chemicals Seelze GmbH*) and $CaCl_2$ (*Honeywell Specialty Chemicals Seelze GmbH*). The ionic strength of the different electrolyte solutions was set to I_m (NaCl) = 0.1 m, 1.02 m, 5.05 m and I_m ($CaCl_2$) = 0.1 m, 1.02 m, 5.36 m, respectively, which in the case of $CaCl_2$ correspond to c ($CaCl_2$) = 0.03 m, 0.34 m and 1.75 m. The stock solutions were prepared by dissolving defined amounts of NaCl or $CaCl_2$ in ultrapure water, which was generated by a Milli-Q® system of Millipore (resistance 18.2 MΩ/cm). The ultrapure water underwent argon-gas purging for 3 h to eliminate dissolved O_2 and CO_2 before transfer into

the glovebox. EDTA ([EDTA] = 10^{-4} M – 10^{-2} M) was added as Na_2H_2EDTA (*Sigma-Aldrich*).

The Europium stock solution was prepared by spiking inactive Eu(III) (c = 10^{-2} M) with ^{152}Eu(III) (*Eckert & Ziegler*). The total Eu(III) concentration for each sample was set to $[Eu(III)]_{tot} = 2{\cdot}10^{-8}$ M, with an activity of A (^{152}Eu(III)) = 2000 Bq at a sample volume of v_{tot} = 10 mL. For TRLFS measurements a Cm(III) solution with the following isotopic composition was used: ^{248}Cm (89.7 %), ^{246}Cm (9.4 %), ^{243}Cm (0.4 %), ^{244}Cm (0.3 %), ^{245}Cm (0.1 %), ^{247}Cm (0.1 %). For every sample the total Cm(III) concentration was set to $[Cm]_{tot} = 1.0{\cdot}10^{-7}$ M. To prepare the C–S–H phases, $CaCO_3$ (*Alfa Aesar*) was calcined to CaO and mixed with SiO_2 (*Aerosil 200, Evonik*) in 50 mL HDPE-vials (*Thermo Fisher Scientific, Sarstedt^{TM}*). The detailed preparation process is described in the subsequent Section.

2.1.1. Synthesis of C–S–H phases

All C–S–H phases were prepared as previously described in the literature (Myers et al., 2015). Hereby $CaCO_3$ was calcined in a furnace at 1000 °C for 12 h, which resulted in CaO. This was followed by direct synthesis of C–S–H phases by mixing CaO and SiO_2 in ultrapure water with the target C/S ratios 0.6, 1.1, 1.4 at a constant solid-to-liquid ratio (S/L) of 20 g/L. C–S–H phases were then equilibrated for 6 weeks before being used for characterization and further experiments. C–S–H phases in NaCl and $CaCl_2$ solutions were prepared at S/L = 1 g/L. A volume of 0.5 mL of the original C–S–H suspension (20 g/L) was contacted with 9.5 mL of NaCl or $CaCl_2$ solutions with the target salt concentration, and equilibrated for 7 days before the addition of the RN or EDTA. The final C/S ratios of the investigated C–S–H phases were determined by considering the initial weight of CaO and SiO_2, as well as the concentrations of [Ca] and [Si] in solution as quantified by ICP-OES (NaCl systems) or estimated ($CaCl_2$ systems, see below). Due to the low S/L ratio in the sorption experiments containing NaCl and $CaCl_2$, the C/S ratio was lower than the original target value, especially in the case of C/S = 1.4 in NaCl due to the greater dissolved concentration of Ca in the aqueous phase (see Section 3.1). The high relative Ca concentration in the aqueous phase of the sorption experiments in $CaCl_2$ prevented the recalculation of the C/S ratio on the basis of the experimentally measured [Ca] and [Si]. Instead, the [Ca] dissolved from the C–S–H phases equilibrated in $CaCl_2$ was calculated by considering the [OH^-] before and after the dilution of the original C–S–H suspension in $CaCl_2$, and assuming that 1 mol of Ca is dissolved per each two mols of OH^-. In combination with the experimentally measured [Si], the estimated [Ca] allowed the calculation of the C/S ratios in the $CaCl_2$ systems. These values must be considered as a semi-quantitative estimation of the real C/S ratio in these C–S–H systems. No Si measurements were conducted in $CaCl_2$ systems with I_m = 1.02 and 5.35 m. Thus, the C/S ratio for these systems could not be calculated, and has been instead assumed the same as for the system with I_m ($CaCl_2$) = 0.1 m.

2.2. Methods

2.2.1. pH measurements in saline solutions

The pH measurements of solutions at high ionic strengths ($I_m \geq 0.1$ m) require the use of a correction factor (A-value), which entails both the activy coefficient of H^+ and the liquid junction potential of the electrode for the given electrolyte type and concentration. The relationship between the corrected pH (pH_m) and the experimentally determined pH value (pH_{exp}) is expressed as follows (1):

$$pH_m = -\log [H^+] = pH_{exp} + A_{salt} \quad (1)$$

The A-values empirically determined for NaCl and $CaCl_2$ solutions are available in the literature (Altmaier et al. 2003, 2008). In the present work, a semi-micro pH electrode (*Orion Ross ultra combination* pH *electrode, Thermo Fisher Scientific, Waltham, Massachusetts)* combined with a Orion Star pH meter (*Orion720 A+)* was used. The electrode was calibrated daily with buffer solutions of pH 3, 6, 8 and 11 (*Certipur® buffer, Merck; Darmstadt, Germany)*.

A summary of the pH values determined in the present work is shown in the Supplementary material (Section A.1, Table S-1 (absence of EDTA) and Table S-2 (presence of EDTA). For a better representation of the tables, the target C/S ratios are used. The results showed increasing pH values from ~10 to ~12.5 with increasing C/S ratio, which is in line with literature data (Häußler et al., 2018; Tits et al., 2006). It is well known that as the C/S ratio increases, the Ca content of the C–S–H phase increases while the Si content decreases. Correspondingly, the pH value increases with the C/S ratio (Lothenbach and Nonat 2015; Yan et al., 2022).

No significant impact of the different electrolyte solutions, the various ionic strengths, the contact times or the presence or absence of the ligand on the pH was detected on the C–S–H phases prepared in the frame of this work.

2.2.2. Characterization of the aqueous phase

[Si] and [Ca] of the aqueous phase equilibrated with C–S–H phases were measured by Inductively Coupled Plasma Optical Emission spectroscopy (ICP-OES, *Avio550 Max*, *PerkinElmer*). To conduct these measurements, the respective C–S–H phases were equilibrated in ultrapure water and NaCl solutions of different ionic strengths in the presence ([EDTA] = 10^{-2} and 10^{-4} M) and absence of EDTA over a period of 7 and 50 d. Subsequently, the solid phase was separated from the liquid phase by ultracentrifugation (1 h, 90 000 rpm). The resulting samples were then diluted in 2 % ultrapure HNO_3 (*Sigma-Aldrich*). The [Si] and [Ca] measured in solution were considered to determine the C/S ratio of the solid C–S–H phase after equilibration with NaCl solutions, as described in Section 2.1.1. Experimentally measured Ca and Si concentrations are provided in the Supplementary material (see Section B.1, Fig. S-1 and S-2). Based on these data, species calculations were performed with the software PHREEQ-C v3.7.3 with adapted Notepad++ and the database ThermoChimie (see Supplementary Material, Figs. S–3) (Parkhurst and Appelo 2013; Giffaut et al., 2014).

2.2.3. Characterization of the solid phase

X-Ray powder diffraction (XRD) measurements were conducted using a D8 Advance (*Bruker*) diffractometer with instrument features such as a Cu K-α radiation source (λ = 0.15418 nm, I = 25 mA, U = 40 kV) and an energy dispersive detector (*Sol-X*). A step width of 0.013° and a step counting of 0.5 s was selected, with 2θ ranging from 10 to 80°. Prior to measurements, each sample was cleaned according to Bernard et al., (2017). Subsequently, the samples were dried for three days in a glovebox under Ar-atmosphere. To maintain an inert atmosphere for the samples, a dedicated sample holder was employed. The sample was positioned on a single crystal silicon wafer, and a cap was placed on top of the silicon wafer to prevent the sample from interacting with air. Data treatment was conducted using the software programs DIFFRAC. EVA version 3.0 (*Bruker*). The Scherrer equation was used to determine the crystallite size, which gives insight into the cristallinity of the C–S–H phases (see Supplementary Material Table S-7 and S-6).More detailed information about the Scherrer equation are given in the literature (Monshi et al., 2012). The measurements were performed for C–S–H phases with C/S ~1.0 in NaCl and $CaCl_2$ solutions of different ionic strength in absence and presence of [EDTA] = 10^{-4} M – 10^{-2} M after a contact time of t = 7 d.

2.2.4. Batch sorption experiments

Two types of batch sorption experiments were conducted to investigate the effect of EDTA on the uptake of Eu(III) on C–S–H phases in addition to experiments only with MQ water: (i) Varying ionic strength, I_m (NaCl) = 0.1, 1.02, 5.05 m; I_m ($CaCl_2$) = 0.1, 1.02, 5.36 m, $[EDTA]_{tot}$ = 10^{-4} M – 10^{-2} M; (ii) constant ionic strength, I_m (NaCl/$CaCl_2$) = 1.02 m; [EDTA] = 10^{-5} – 10^{-2} M. The following boundary conditions were used for each experiment: Solid-to-liquid-ratio $(S/L)_{constant}$ = 1 g/L,

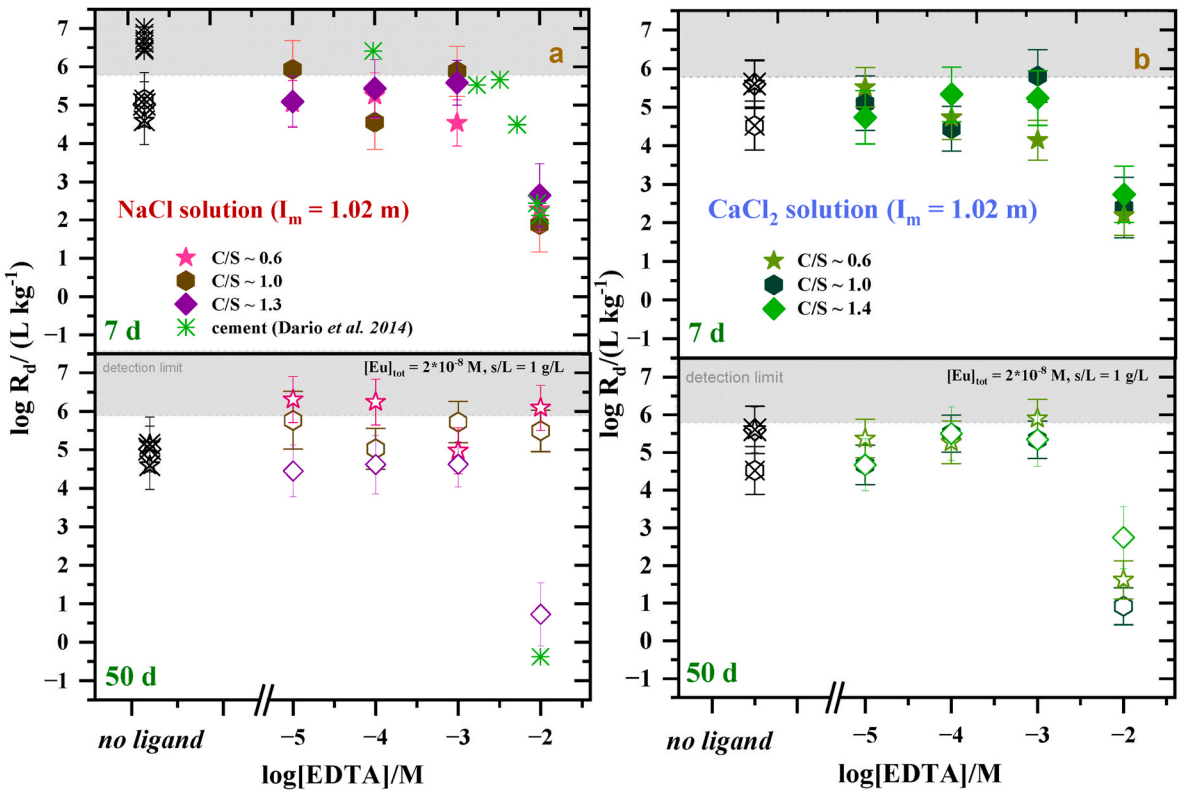

Fig. 1. (a) Distribution coefficients (log R_d/L kg^{-1}) as determined in this work for the sorption of Eu(III) on C–S–H phases for different C/S ratios ranging between ~ 0.6 and 1.3 at varying [EDTA] = 10^{-5} - 10^{-2} M in NaCl solutions (I_m = 1.02 m) after sorption times of 7 d (top) and 50 d (bottom). The results are obtained at S/L = 1 g/L and $[Eu]_{tot}$ = 2·10^{-8} M. The Figure includes also data reported by Dario *et al.* for the uptake of Eu(III) by Portland cement at pH = 12.5 in the presence of increasing concentrations of EDTA after 7 and 50 d (Dario et al., 2004) (b) Distribution coefficients (log R_d/L kg^{-1}) for the sorption of Eu(III) on C–S–H phases for different C/S ratios ranging between ~ 0.6 and 1.4 at varying [EDTA] = 10^{-4} M - 10^{-2} M in $CaCl_2$ solutions (I_m = 1.02 m) after sorption times of 7 d (top) and 50 d (bottom).

sorption times of 7 and 50 d and various C/S ratios ranging from ~ 0.6 to 1.4. An additional batch sorption series was carried out in absence of EDTA at a constant ionic strength of I_m (NaCl/$CaCl_2$) = 1.02 m. The general procedure applied for all batch sorption experiments is given in the following: Each sample was prepared in 20 mL-HDPE–bottles (*Zinsser Analytics*). After the specific sorption time, the supernatant was transferred in centrifuge tubes (*Quick-Seal, Beckman Coulter)* and centrifuged at 90 000 rpm for 1 h *(rotor: 90TI, centrifuge: Beckman Coulter OPTIMATM XPN-90*). After centrifugation, an aliquot of the sample was taken and acidified with HNO_3 (65%, *Supelco*). The activity of ^{152}Eu was quantified using a γ-counter (*2480 Automatic Gamma Counter Wizard 2, PerkinElmer*). Measurements were limited to a maximum of 3 h.

All batch sorption experiments were quantified using the distribution coefficient R_d, given in L/kg. It describes the relationship between the concentration of the adsorbed species and the concentration of the species in solution, as given in equation (2):

$$R_d = \frac{(C_{init} - C_{aq})}{C_{aq}} * \frac{V}{m} \quad (2)$$

The initial concentration of the adsorbed species is given by C_{init}, and the concentration of the aqueous species is given with C_{aq}. V is the volume of the liquid phase, while m is the mass of the solid phase. The limit of detection for ^{152}Eu(III) by γ-counter in the conditions of this study was 2.0·10^{-11} M, quantified as three times the standard deviation of blank samples. Considering the initial concentration of ^{152}Eu(III) and the S/L ratio used in these experiments, this results in an upper limit for the distribution coefficient of log $R_{d,max}$ ~ 6. Adsorption of Eu(III) to the walls of the HDPE vials can most probably be disregarded in our calculations. Due to the high saline conditions of our samples, sorption effects to the walls are considered to be minimized.

2.2.5. TRLFS experiments

TRLFS measurements were conducted using a Nd:YAG laser (*Continuum Surelite II*) coupled to a dye laser system (*Radiant dyes Narrow Scan, Dye: Exalite 398*) with an energy output ranging from 1 to 4 mJ. The dye laser was tuned to a wavelength of λ = 396.6 nm, corresponding to the most intensive absorption band of the Cm(III) ion. Additional details on the spectroscopic properties of Cm(III) are presented in the literature (Tits et al., 2003; Fanghänel and Kim 1998).

The emission spectra were recorded with an optical multichannel analyzer connected to a polychromator unit (*Shamrock 303i, Andor)* and an ICCD-camera (*iStar, Andor; Modell DH720- 18F-63*). An optical grating with 1200 lines mm^{-1} was used for the spectra resolution, resulting in a detectable wavelength range of = 590–640 nm. Emission spectra were obtained after 1 μs of delay time after the laser pulse and with a time window of 1 ms. The intensity measured is divided by the laser energy, thereby normalizing the spectrum to the laser energy. Fluorescence lifetimes were aquired by measuring series of emission spectra with increasing delay time. All samples were prepared at a constant S/L = 1 g/L, contact times of up to 365 d, constant I_m (NaCl or $CaCl_2$) = 1.02 m and varying $[EDTA]_{tot}$ = 10^{-4} – 10^{-2} M.

Due to the similar results obtained in sorption experiments with C–S–H phases of C/S ~ 0.6 and ~ 1.0 (see Section 3.3), TRLFS measurements focussed on the systems with C/S ~ 1.0 (NaCl and $CaCl_2$) and C/S ~ 1.3 (NaCl) and 1.4 ($CaCl_2$) (final C/S ratios depending on the salt and EDTA concentrations, see Sections 2.2.2 and 3.1). TRLFS measurements for each sample were conducted in both the solution and suspension. Solution samples were measured after phase separation by sedimentation. The suspension samples were measured under

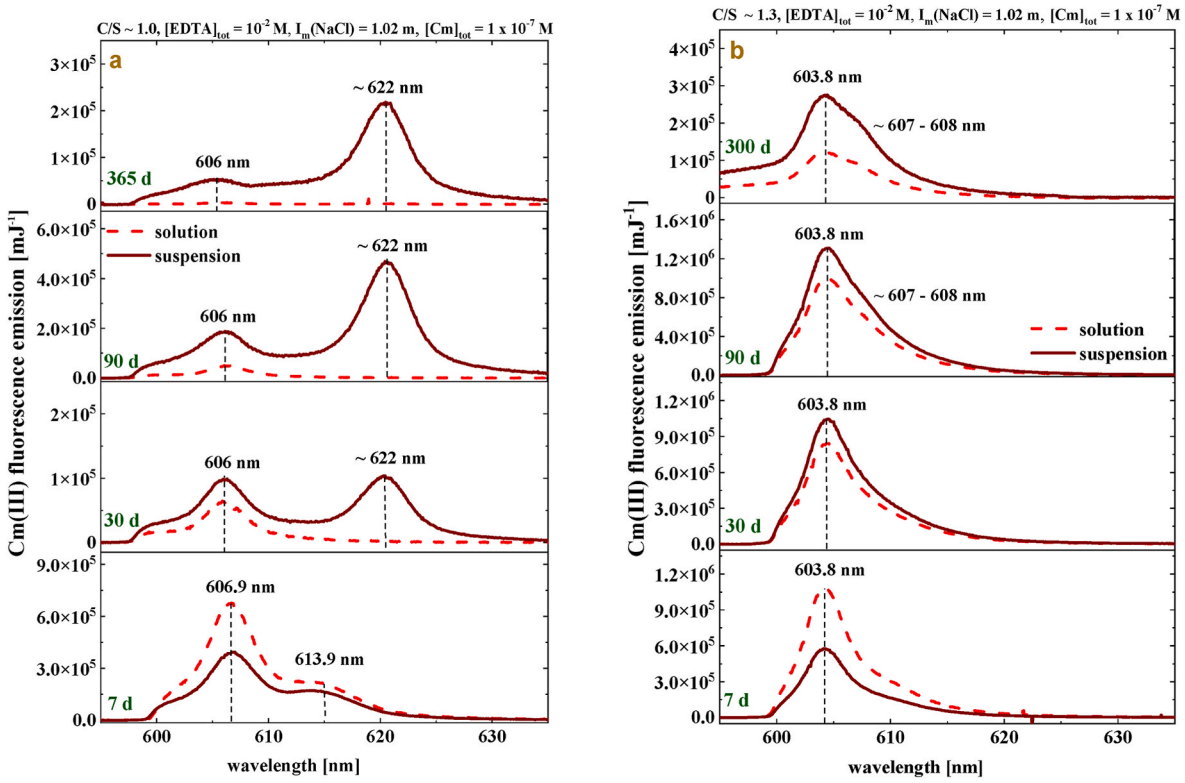

Fig. 2. Fluorescence emission spectra: Cm(III) ($[Cm]_{tot} = 1{\cdot}10^{-7}$ M) in the presence of C–S–H phases and [EDTA] = 10^{-2} M with (a) C/S ~ 1.0 and (b) C/S ~ 1.3 in NaCl solution ($I_m = 1.02$ m) up to 365 d of contact time. All measurements are conducted in the supernatant (light red dots) and the suspension (dark red line) at S/L = 1 g/L.

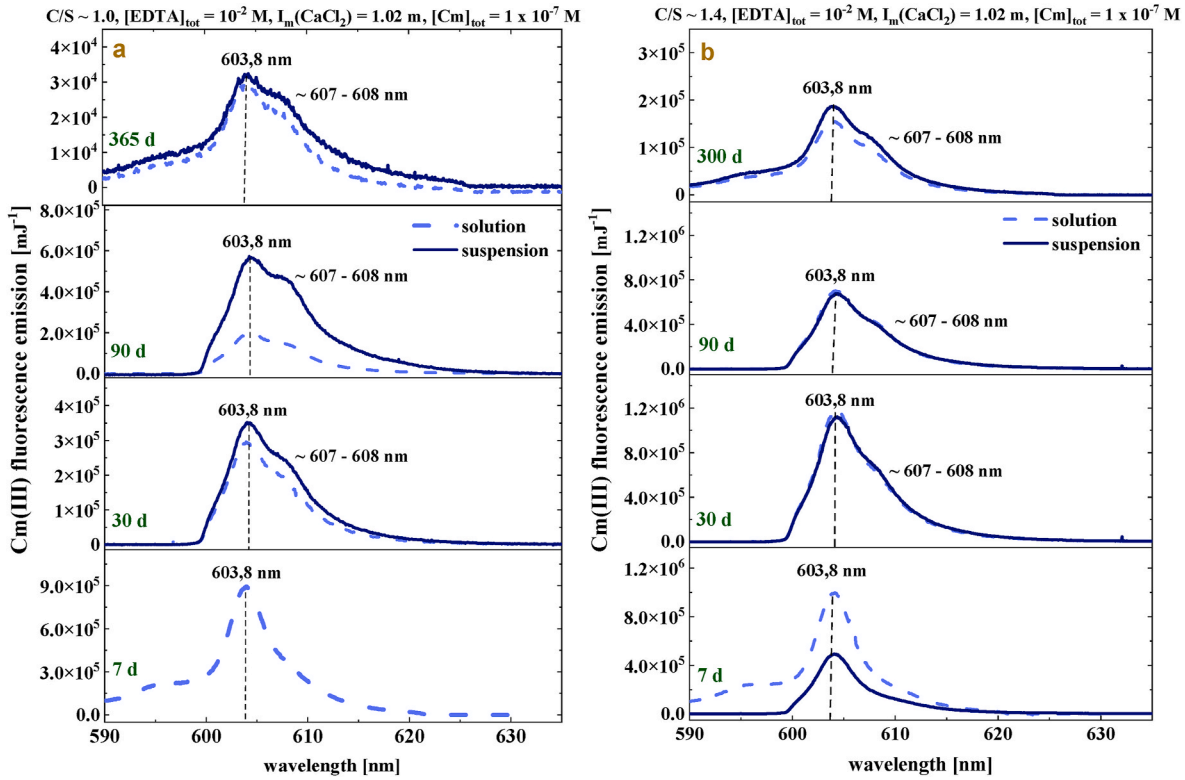

Fig. 3. Fluorescence emission spectra: Cm(III) ($[Cm]_{tot} = 1{\cdot}10^{-7}$ M) in the presence of C–S–H phases and [EDTA] = 10^{-2} M with (a) C/S ~ 1.0 and (b) C/S ~ 1.4 in $CaCl_2$ solution ($I_m = 1.02$ m) up to 365 d of contact time. All measurements are conducted in the supernatant (light blue dots) and the suspension (dark blue line) at S/L = 1 g/L.

continuous agitation with a stirring bar, in order to ensure the homogeneity of the sample. In between the measurements, the samples were removed from the quartz cuvette and stored under argon atmosphere in 15 mL polypropylen (PP) tubes (*Sarstedt*).

3. Results and discussion

3.1. Determination of [Ca] and [Si] in presence and absence of EDTA

The concentrations of Ca and Si of the aqueous solutions in contact with the C–S–H phases were determined both in the presence and absence of EDTA, and for two different contact times of 7 and 50 d in NaCl solutions.

A detailed overview of measured [Ca] and [Si] in solutions from different experiments is provided in the Supplementary material (Section B.1, Fig. S-1 and Fig. S-2). The corresponding C/S ratios in C–S–H phases contacted with NaCl and $CaCl_2$ can also be found in the Supplementary material (Section B.1, Table. S-3 and S-4).

In absence of EDTA, [Ca] increases slightly with the C/S ratio of the C–S–H phase contacted with NaCl solution for all ionic strength at t = 7 days. The [Ca] increases with increasing C/S ratio, which is in line with literature data (Lothenbach and Nonat 2015). The data after 50 d of sorption time are similar to those obtained after 7 d. There is no significant effect of the different ionic strength of NaCl observed on the C–S–H phase.

In NaCl systems containing [EDTA] = 10^{-2} M, the trend of increasing [Ca] with increasing C/S ratio is very clear for all equilibration times (Figs. S–1 in the Supporting Material). At short and long equilibration times (t = 7 and 50 days), the Ca concentrations measured in the presence of EDTA are significantly higher than in EDTA-free systems. This is consistent with the expected formation of the stable complex $Ca(EDTA)^{2-}$ (Hummel et al., 2005). At both equilibration times, this does not have a significant effect on the C/S ratio (see Table S-3 and S-4 in the Supporting Information). To reiterate the importance of [Ca], these are discussed in more detail at the end of Section 3.4.

As discussed in Section 2.1.1, the large excess of added Ca in $CaCl_2$ solutions prevents the analysis of Ca dissolving from C–S–H phases and, thus, the accurate determination of final C/S ratios. Instead, orientative estimates are provided in the Supplementary material at an ionic strength of I_m = 0.1 m in presence and absence of EDTA (Section B.1, Tables S–4). The tentatively determined C/S ratios for $CaCl_2$ solutions are very similar to those in NaCl at C/S ~ 0.6 and C/S ~ 1.0. Only the highest C/S ratios show a slight deviation (C/S ~ 1.3 in NaCl and C/S ~ 1.4 in $CaCl_2$). Since the results in NaCl show only a minor effect of the ionic strength on the C/S ratio, this is also assumed for the $CaCl_2$ systems. Accordingly, the C/S ratios in $CaCl_2$ solution are given as C/S ~ 0.6, C/S ~ 1.0 and C/S ~ 1.4 in the following.

3.2. Characterization of the solid C–S–H phases in presence and absence of EDTA

The impact of EDTA on the C–S–H phases was studied by XRD. The respective XRD spectra at EDTA = 10^{-4} – 10^{-2} M and at different ionic strenghts are given in the Supplementary material (Section C.1, Fig. S-4 and Fig. S-5).

In absence of EDTA, the XRD pattern are characteristic for C–S–H phases and show broad signals at 2θ = 8°, 29.1°, 32°, 50° and 55°. This is in excellent agreement with literature data, clearly showing the successful synthesis of the C–S–H phases (Grangeon et al., 2013; Barzgar et al., 2020; Lothenbach and Nonat 2015; Häußler et al., 2018; Garbev et al., 2008; Maragkou and Pashalidis 2021; Nonat 2004). For all solid phases with different C/S ratios, the structure can be assigned to Tobermorite 14 Å according to Taylor et al. (Taylor 1986). Furthermore, no residues of NaCl, $CaCl_2$ or portlandite are observed, demonstrating the appropriate cleaning of the solid phase prior to XRD analysis. For C–S–H phases equilibrated in NaCl and $CaCl_2$ solutions at I_m = 0.1 m, the intensities of the signals are similar compared to those in ultrapure-water. For higher ionic strengths, however, the intensities decrease distinctively both in NaCl and $CaCl_2$ solutions. Apparently, contact with high ionic strength NaCl solutions results in less ordered structures of the C–S–H phase, with unevenly distributed interlayers and layer spacing independent of the electrolyte cation (Häusler 2023). The XRD pattern for C–S–H phases in presence of [EDTA] ≤ 10^{-3} M are in good agreement to those in absence of the ligand and, thus, do not show an effect on the solid C–S–H phase structure.

At [EDTA] = 10^{-2} M, the intensities of the typical signals of the C–S–H phase are decreased compared to EDTA-free systems. This might be explained by the slight dissolution of the C–S–H material observed at this ligand concentration. In spite of this, the crystallinity degree of the solid phase is not significantly affected, as calculated with the Scherrer equation in terms of the crystallite size (Monshi et al., 2012). For the C–S–H phases in NaCl and $CaCl_2$ solutions, particle sizes between 9 and 11 nm were determined for all EDTA concentrations (see Supplementary Material Table S-7 and S-6).

A new feature is also observed at 2θ = 28.16° in the EDTA-containing samples. The signal is weak at low [EDTA] ≤ 10^{-3} M and becomes more prominent at [EDTA] = 10^{-2} M. The solubility of $Ca_2(EDTA)\bullet 7H_2O$(cr) in dilute to concentrated NaCl solutions has been reported to range between 0.035 M and 0.06 M (in terms of EDTA concentration) (Xiong et al., 2017). We speculate that this solid may have formed in the process of drying the C–S–H phases, eventually involving EDTA sorbed on the C–S–H surface. Experimental XRD data for longer sorption times are currently not available. However, the batch sorption and TRLFS results clearly showed the presence of C–S–H phase, even after 365 days of equilibration time. A clear incorporation of Eu(III)/Cm(III) into was observed, if no strong ternary or quaternary complexes stabilizes the metal ion in solution, indicating that the C–S–H phase is present with its defined mineral structure. Hence, it is assumed that the structure of the C–S–H phase does not change significantly over time.

3.3. Batch sorption experiments: effect of ionic strength and [EDTA]

The uptake of Eu(III) on C–S–H phases in presence of [EDTA] = 10^{-4} and 10^{-2} M was initally investigated in NaCl and $CaCl_2$ electrolyte solutions of varying ionic strength (0.1 m ≤ I_m ≤ 5.05 m). The corresponding data are summarized in the Supplementary Information, Section D.1, Fig. S-6 and Fig. S-7. The results showed no significant differences between the experimental series at different ionic strength, and thus the results discussed in this Section focus only on data obtained at a constant ionic strength of I_m = 1.02 m.

The uptake of Eu(III) by C–S–H phases in the absence and presence of [EDTA] (10^{-4} – 10^{-2} M) at t = 7 and 50 d is shown in Fig. 1a (NaCl systems) and Fig. 1b ($CaCl_2$ systems). Very high distribution ratios (4.5 ≤ log R_d ≤ 5.5, with R_d in $L\bullet kg^{-1}$) are quantified for the uptake of Eu(III) by C–S–H phases in the absence of EDTA, in both electrolytes. In NaCl as well as $CaCl_2$ solution with [EDTA] ≤ 10^{-3} M, similar high retention with log R_d = 4–6 (with R_d in $L\bullet kg^{-1}$) is observed after 7 and 50 d for all C/S ratios. This reflects a negligible effect of EDTA on the Eu(III) uptake by C–S–H phases in this range of ligand concentrations.

At [EDTA] = 10^{-2} M, the uptake of Eu(III) by C–S–H phases in NaCl solution with C/S ratios of ~ 0.6 and ~ 1.0 is significantly decreased after a contact time of 7 d, but increases again to log R_d ~ 4–5 at t = 50 d. In contrast to these observations, at C/S = 1.3, the log R_d values remain low after 50 d. In $CaCl_2$ solutions, at [EDTA] = 10^{-2} M, low log R_d ~ 2–3 are observed for all investigated systems. A detailed explanation on these effects is given in section 3.4.

Fig. 1a also shows the results obtained by Dario and co-workers for the uptake of Eu(III) by Portland cement in the presence of increasing EDTA concentrations (Dario et al., 2004). The experiments were performed at pH ~ 12.5 and S/L = 1 g/L. Although with slightly higher pH and expectedly higher C/S ratio in the C–S–H phases, the results obtained by Dario et al. are in good agreement with the data obtained in

the present work for the C–S–H systems at 7 and 50 d (Dario et al., 2004). The log R_d value obtained after 50 d for Dario et al. with log $R_d \sim -0.54$ is slightly lower than for the present system with log $R_d \sim 1$. This is due to the fact that these are two similar but not identical systems, which makes a direct comparison impossible. Nevertheless, the data are in very good agreement.

These results for C/S ~ 1.3 (NaCl) and all investigated C/S ratios in $CaCl_2$ solution, strongly support the formation of stable complexes of Eu (III)-EDTA under the hyperalkaline conditions defined by C–S–H phases and with high ligand concentrations ([EDTA] $> 10^{-3}$ M). Ca forms rather strong complexes with EDTA, (Hummel et al., 2005) resulting in a limited concentration of free EDTA available to bind lanthanides or actinides. Following this reasoning, EDTA complex formation of lanthanides and actinides in presence of high Ca-concentrations should be of low relevance. The sorption experiments conducted in this work in $CaCl_2$ solutions clearly disregard this hypothesis, providing indirect evidence on the formation of ternary or quaternary complexes involving Ca, *i.e.*, Ca–Eu(III)-EDTA or Ca–Eu(III)–OH-EDTA. Note that the effect of EDTA in NaCl solutions is only observed when in contact with C–S–H phases with higher C/S > 1.0 and Ca concentrations in the porewater are elevated, or in cement systems with pH ~ 12.5 (Dario et al., 2004). The formation of analogous complexes for *An* (III) was recently proposed by DiBlasi and co-workers on the basis of solubility, TRFLS experiments and quantum chemistry calculations with Pu(III) and Cm(III), respectively (DiBlasi et al., 2022).

3.4. Spectroscopic characterization of Cm(III) on C–S–H phases in presence of EDTA

The emission spectra of Cm(III) in presence of C–S–H phases, [EDTA] = 10^{-2} M and I_m = 1.02 (NaCl) are displayed in Fig. 2a and b for C–S–H phases with C/S ~ 1.0 and ~ 1.3, respectively, after different contact times. The Figures show the measurements of the suspensions under continuous agitation (solid lines), as well as for the supernatant solution after phase separation by sedimentation (dashed lines) (see Section 2.2.5). The measurements of the fluorescence lifetimes for all systems are given in Table 1.

At C/S ~1.0, two main emission bands at 606.9 and 613.9 nm are detected after 7 d. These bands are visible in the supernatant, as well as in suspension. The fluorescence lifetime of the former signal is determined to be 280 ± 11 μs in solution, whereas 315 ± 20 μs is observed in suspension. If the suspension contains surface adsorbed Cm(III) species, this would indicate that these species are the same as the solution species. However, the present data set does not allow a clear distinction between surface bound or aquatic species. The signal at 613.9 nm reveals a fluorescence lifetime of 164 ± 14 μs (Table 1) in solution. These results are in good agreement with previous observations that attributed these bands to two different Cm(III) species: $Cm(OH)(EDTA)^{2-}$ (at 606.9 nm) and $Cm(OH)_x(EDTA)^{-(x+1)}$ (at 613.9 nm) (DiBlasi et al., 2022).

After 30 d of contact time, the emission bands at 606.9 and 613.9 nm disappear and two new peaks are formed at 606- and 620.9 nm. The latter band is only visible in suspension. Additionally, the band shifted slightly towards higher wavelength of ~ 622 nm with increasing contact time. A lifetime of 1317 ± 21 μs (Table 1) averaged for the different contact times is determined for this band. In this context, the Kimura equation can be applied to establish a correlation between the fluorescence lifetime and the number of coordinated water molecules in the first coordination sphere of the Cm aquo-ion (Kimura and Choppin 1994). On this basis, the long lifetime measured after 50 days corresponds to a species with no inner-sphere bound water molecules associated and a strong ligand field splitting. Hence, it is assigned to an incorporated species of Cm(III) into the CaO-layer of the C–S–H phase, as previously described in the literature (Tits et al., 2003) The peak at 606 nm represents a hot band of this species (Tits et al., 2003). This is due to the thermal population of the higher ligand field levels of the Cm_{aq} ion. A detailed explanation can be found elsewhere (Edelstein et al., 2006; Carnall 1992).

At C/S ~ 1.3, a main emission band at 603.8 nm is detected for all contact times up to 300 d in solution and suspension (see Fig. 2b). The fluorescence lifetime of this band does not change significantly over the studied contact time, and averaged lifetimes of 163 ± 12 μs in solution, and 158 ± 15 μs in suspension were determined (see Table 1). According to DiBlasi *et al.*, this band is attributed to the ternary Ca–Cm(III)-EDTA complex, which can form due to the increased calcium concentration originating from the higher C/S ratio (DiBlasi et al., 2022). Furthermore, a slight shoulder between 607 and 608 nm in solution and suspension spectra is visible for contact times of t > 90 d. This emission band lies close to that observed by DiBlasi et al., (2022), who assigned the corresponding species to the quaternary Ca–Cm(III)–OH-EDTA complex. However, luminescence lifetime was much higher (τ = 813 ± 280 μs) and the respective spectrum was only observed at pH > 12, whereas the pH of this sample is significantly lower at pH = 11.3. Thus, at the current state of knowledge, the formation of this shoulder can not be fully explainend. In comparison to experiments performed with C–S–H with C/S ~ 1.0, there is no incorporation of Cm(III) in the C–S–H phase with C/S ~ 1.3 visible within one year.

The TRLFS data for both C/S ratios are in excellent agreement to the corresponding batch sorption experiments. While consistently strong retention of Eu/Cm(III) is observed for experiments with C–S–H phases with C/S ~ 1.0 in batch and TRLFS studies, low sorption is found for C/S ~ 1.3 with a log R_d = 1 for Eu(III). This corresponds to about 99 % of Eu/Cm(III) remaining in solution and explains that Cm(III)-TRLFS spectra for suspension and solution species are virtually identical. Hence, the increase of Ca in the solution due to the higher C/S ratio results in the

Table 1
Peak positions (nm) and fluorescence lifetimes (μs) of the Cm(III) uptake on C–S–H phases (C/S ~ 1.0 and ~1.3, ~1.4) in NaCl and $CaCl_2$ solutions (I_m = 1.02 m). Sorption times between 7 and 365 d are considered for all the systems. Additionally literature data is included (DiBlasi et al., 2022; Tits et al., 2003). Due to the minor changes of some fluorescence lifetimes with different sorption times, average lifetimes are calculated. These are underlined.

Species	Band (nm)	Contact time (d)	pH_m	Lifetime supernatant (μs)	Lifetime suspension (μs)	Lifetime solution Lit./(μs)
C/S ~1.0 - NaCl solution, [EDTA] = 10^{-2} M						
$Cm(OH)(EDTA)^{2-}$	606.9	7	11.2	280 ± 11	315 ± 20	331 ± 41
$Cm(OH)_x(EDTA)^{-(x+1)}$	613.9	7	11.2	164 ± 14	–	173
Incorporation species	~622	>30	11.1	–	1317 ± 21	1480 ± 200
C/S ~1.3 - NaCl solution, [EDTA] = 10^{-2} M						
Ca-Cm-EDTA	603.8	7–300	11.1	163 ± 12	158 ± 15	151
$Cm(OH)(EDTA)^{2-}$	606.9	7–300	11.1	–	-	331 ± 41
C/S ~1.0 – $CaCl_2$ solution, [EDTA] = 10^{-2} M						
Ca-Cm-EDTA	603.8	7–365	10.8	166 ± 12	162 ± 18	151
$Cm(OH)(EDTA)^{2-}$	606.9	7–365	10.8	–	-	331 ± 41
C/S ~1.4 – $CaCl_2$ solution, [EDTA] = 10^{-2} M						
Ca-Cm-EDTA	603.8	7–365	10.9	167 ± 14	172 ± 12	151
$Cm(OH)(EDTA)^{2-}$	606.9	7–365	10.9	–	-	331 ± 41

formation of the very stable Ca–Cm(III)-EDTA species, which stabilizes the trivalent actinide in solution. We acknowledge that the sharp change in the retention and overall Eu/Cm speciation caused by the relatively small increase in the [Ca] arising between the porewater of C–S–H with C/S ~ 1.0 and ~ 1.3 (see Tables S–3) is a priori unexpected. Note however that besides [Ca], also pH and C/S ratio (*i.e.*, surface properties) are modified, possibly reflecting that this is the result of the coupling of different processes. In the same line, Dario *et al.* reported a sharp decrease in the distribution ratio of Eu(III) (from log R_d ~ 5.5 to R_d ~ 2) for a slight increase in the EDTA concentration of 0.5 $\log_{10}$-unit, *i.e.*, from $10^{-2.5}$ to 10^{-2} M (see Fig. 1a) (Dario et al., 2004). This observation is further discussed below in connection with the results obtained for the $CaCl_2$ system.

Fluorescence emission spectra of Cm(III) in the presence of C–S–H phases and [EDTA] = 10^{-2} M in $CaCl_2$ solutions are displayed in Fig. 3a for C/S ~ 1.0 and Fig. 3b for C/S ~ 1.4. Hereby, contact times between 7 and 365 d were studied.

For both C/S ratios, a primary emission band at 603.8 nm is visible in solution and suspension for all contact times. In both cases the fluorescence lifetimes averaged for all contact times are identical within the experimental uncertainty (166 ± 12 μs in solution, and 162 ± 18 μs in suspension). This signal is again attributed to the ternary Ca–Cm(III)-EDTA complex (DiBlasi et al., 2022). For longer sorption times of t > 30 d, a shoulder appears with a wavelength of around 607–608 nm, which may be attributed to a quaternary Ca–Cm(III)–OH-EDTA species (see discussion above). The absence of a band around 621–622 nm clearly shows, that no incorporation of Cm(III) into the C–S–H phase takes place under these conditions. Again TRLFS and batch sorption experiments are consistent by showing both a low retention of Eu/Cm(III) under these conditions.

The results obtained in $CaCl_2$ solutions are key for the correct interpretation of the underlying retention mechanims. Dario et al. and Ochs *et al.* argued that the predominance of the Ca $(EDTA)^{2-}$ complex dramatically decreased the free ligand concentration, and that the decrease in the R_d values observed by the former only occurred when the concentration of EDTA was above the concentration of Ca in the porewater (Dario et al., 2004; Ochs et al., 2022). Indeed, similar observations have been obtained in this work for the C–S–H system with C/S ~ 1.3 equilibrated in NaCl solution at I_m = 1.02 m. However, this argument does not hold for the $CaCl_2$ systems, where Ca is in all cases in large excess with respect to EDTA. Hence, the observed decrease in the uptake of Eu(III) occurring in $CaCl_2$ can only be explained by the formation of ternary or quaternary complexes involving Ca, *i.e.*, Ca–Eu(III)-EDTA or Ca–Eu(III)–OH-EDTA. Differences in the aqueous speciation are confirmed by TRLFS for Cm(III)-EDTA systems with C–S–H ~ 1.0 and ~ 1.3.

The Cm(III) uptake on C–S–H phases was further studied at low EDTA concentrations of 10^{-4} M – 10^{-3} M in NaCl and $CaCl_2$ solutions for sorption times between 7 and 365 d. The corresponding spectra are given in the Supplementary material (Section E.1, Fig. S-8). In both electrolyte solutions, the incorporation of Cm(III) into the C–S–H phase was observed over the studied sorption time. This clearly showed that EDTA in this low concentration range has no significant effect on the Cm (III) sorption on C–S–H phases. The results are in good agreement with the analogous batch sorption data of the present work, and with literature data (Tits et al., 2003).

At this point, the changing total emission intensities of the spectra should be mentioned. An important point to consider is that no quantitative phase separation was performed during the TRLFS measurements. The samples were sedimented over the selected time period, and the supernatant was measured first by sampling with a pipette. Afterwards, the supernatant was returned and the sample was shaken, producing a suspension, which again was measured. This procedure was applied to enable a repetitive usage of the same sample for several measurements over a period of one year. Due to this approach, the total emission intensities may exhibit rather large errors or artifacts and should not be overinterpreted.

Hence, the results obtained in the present work can be explained as follows: In NaCl solution for low C/S ~ 1.0 and at all investigated EDTA concentrations up to 10^{-2} M, an initial stabilization of Eu(III) by the formation of Eu(III)–OH-EDTA complexes takes place within a few days of contact time with C–S–H phases, resulting in a reduced sorption of the metal ion to the C–S–H phase. At longer contact times, the thermodynamically favored incorporated species of Eu(III) in the C–S–H phase forms, leading to the observed strong retention. In our experiments incorporation is found at around 50 days of contact time. If Ca is at a sufficiently high concentration, apparently very stable ternary or possible quaternary Ca–Eu(III)–(OH)–EDTA complexes can form, resulting in a strong stabilization of the trivalent actinide or lanthanide in the aqueous phase. This is reflected by the low retention of Eu(III) in $CaCl_2$ dominated solutions, as well as at C/S ~ 1.3 in NaCl solution. In the latter case, the high calcium to silicon ratio results in higher calcium concentrations in the aqueous phase, enabling the formation of the formation of ternary and/or quaternary complexes. In order to better elaborate on this point, the Ca concentrations of the NaCl systems in the absence of EDTA and at [EDTA] = 10^{-2} M are provided in Figs. S–1 in the Supplementary Material.

In absence of EDTA significantly lower [Ca] values are obtained for all C/S ratios, compared the systems in presence of EDTA (see Figs. S–1). The results of the batch and TRLFS experiments in NaCl showed, that at C/S = 1.0 and after 7 d the Ca-free complex Cm-EDTA-OH forms. Contrary, at C/S = 1.3 the ternary complex Ca-Cm-EDTA is the dominant species. Thus, the lower [Ca] and lower pH values present at lower C/S ratio do not enable the formation of a significant amount of the Ca-containing ternary complex. It is worth noting that a relatively small increase in Ca-concentrations (from ~ 7 mM at C/S ~ 1.0and ~ 9 mM at C/S ~ 1.3, see Supplementary Material, Figs. S–2) together with the increased pH (from C/S ~ 1.0 to C/S ~ 1.3, see Supplementary Material, Figs. S–2) is sufficient to induce the predominant formation of those complexes and counteract sorption.

In addition to the determination of Ca-concentrations, the speciation of EDTA in the Na–Ca-EDTA system was calculated and is shown in Figs. S–3 in the Supplementary Material. The strong complex $CaEDTA^{2-}$ dominates the aqueous speciation in presence of [Ca] = 9 mM, whereas the complex $NaEDTA^{3-}$ prevails in Ca-free systems at pH > 9. This is in line with the high stability constant reported for this complex (log K^0 = 12.69 ± 0.06) (Hummel et al., 2005).

For the ternary complexes Ca-Cm-EDTA and Ca–Cm(III)–OH-EDTA, it is not possible to make similar speciation calculation in the present stage, since the thermodynamic data (*e.g.* log K^0) are not yet available. Based on the available batch sorption- and TRLFS data, it is assumed that the ternary Ca–Cm(III)-EDTA and Ca–Cm(III)–OH-EDTA complexes outcompete the $CaEDTA^{2-}$ complex. At this point we want to emphasis that these findings are of preemptive nature and the absolute values should be treated critically. In order to give a resilient discussion on this topic, comprehensive thermodynamic data on the different species is mandatory.

4. Conclusion

The effect of EDTA on the uptake of Eu(III) and Cm(III) on C–S–H phases was investigated from low to high ionic strength in NaCl and $CaCl_2$ solutions. Hereby the combination of classical batch sorption studies and laser spectroscopy contributes to the quantitative description and mechanistic understanding of the complex interaction of trivalent actinides with cementitious systems of relevance for a possible nuclear waste disposal scenario.

At low [EDTA] ≤ 10^{-3} M, strong retention of Eu(III) was displayed for all the investigated systems. Hereby, TRLFS confirmed that this effect is due to the incorporation of Eu(III)/Cm(III) into the C–S–H structure. Hence, EDTA in these concentration does not affect the uptake of Eu(III) and Cm(III) on C–S–H phases under the given conditions.

At [EDTA] = 10^{-2} M, the retention of Eu(III) was significantly decreased in NaCl and $CaCl_2$ solutions at short contact times (t = 7 d). However, almost quantitative Eu(III) retention was displayed at longer contact times (t = 50 d) in the NaCl system at C/S ~ 0.6 and C/S ~ 1.0. For C–S–H phases with C/S ~ 1.3 in NaCl solution as well as for all investigated C/S ratios in the $CaCl_2$ system, a very significant decrease of log R_d values is observed at [EDTA] = 10^{-2} M and t = 7–50 d. This behaviour was explained as follows: At the lower calcium concentrations defined by C–S–H with C/S ≤ 1.0 in NaCl solutions, the presence of EDTA leads to a quick formation of Eu(III)/Cm(III)-EDTA complexes, which initially stabilize the trivalent metal ion in the aqueous phase. However, as the contact time progresses, the Eu(III)/Cm(III) is incorporated into the interlayer of the C–S–H phase, forming the thermodynamically stable species. In the presence of sufficiently high calcium concentrations, *i.e.* for C–S–H with C/S > 1.0 (in NaCl systems) and for all C/S ratios in $CaCl_2$ systems, the formation of ternary complexes Ca–Eu(III)/Cm(III)-EDTA effectively stabilize Eu(III)/Cm(III) in the aqueous phase and suppress the incorporation process effectively at [EDTA] = 10^{-2} M. It is noticeable that this significant change in Eu(III)/Cm(III) speciation and retention behaviour may already occur at even small variations in Ca-concentrations.

This work contributes to the in-depth understanding of the impact of organic complexing agents on the retention trivalent actinides on C–S–H phases on the macro- and molecular scale. The results show the distinct impact of calcium ions, leading to the formation of new actinide/organic species, which may be very stable in the aqueous phase. The presence of this complexes may significantly impact the migration behaviour of trivalent actinides in the near field of a nuclear waste repository, and their comprehensive thermodynamic description can be of high relevance for the safety case of a deep geological waste repository when considering specific scenarios. The observed reactions are virtually independent of ionic strength, so that data are applicable to porewater compositions with low up to intermediate salinity.

Funding

This work was funded by the German Federal Ministry for the Environment, Nature Conservation, Nuclear Safety and Consumer Protection (BMUV) under the contract number 02E11860C (GRaZ II).

CRediT authorship contribution statement

Aline K. Thumm: Writing – review & editing, Writing – original draft, Investigation, Formal analysis, Data curation, Conceptualization. **Andrej Skerencak-Frech:** Writing – review & editing, Supervision, Project administration, Conceptualization. **Xavier Gaona:** Writing – review & editing, Supervision, Conceptualization. **Marcus Altmaier:** Writing – review & editing, Supervision, Project administration, Funding acquisition. **Horst Geckeis:** Writing – review & editing, Supervision.

Declaration of competing interest

The authors declare the following financial interests/personal relationships which may be considered as potential competing interests: Karlsruhe Institute of Technology (KIT), Institute of Nuclear Waste Disposal (INE) reports financial support was provided by German Federal Ministry for the Environment, Nature Conservation, Nuclear Safety and Consumer Protection (BMUV). If there are other authors, they declare that they have no known competing financial interests or personal relationships that could have appeared to influence the work reported in this paper.

Data availability

Data will be made available on request.

Acknowledgements

The authors would like to thank Stephanie Kraft at KIT-INE for her dedicated efforts in collecting the ICP-OES results.

Appendix A. Supplementary data

Supplementary data to this article can be found online at https://doi.org/10.1016/j.apgeochem.2024.106087.

References

Altmaier, M., Metz, V., Neck, V., Müller, R., Fanghänel, T., 2003. Solid-liquid equilibria of $Mg(OH)_2$ (cr) and $Mg_2(OH)$ 3Cl $4H_2O$ (cr) in the system Mg-Na-H-OH-Cl-H2O at 25 C. Geochim. Cosmochim. Acta, GCA 67, 3595–3601.
Altmaier, M., Neck, V., Fanghänel, T., 2008. Solubility of Zr (IV), Th (IV) and Pu (IV) hydrous oxides in CaCl2 solutions and the formation of ternary Ca-M (IV)-OH complexes. Radiochim. Acta 96, 541–550.
Barzgar, S., Lothenbach, B., Tarik, M., Di Giacomo, A., Ludwig, C., 2020. The effect of sodium hydroxide on Al uptake by calcium silicate hydrates (CSH). J. Colloid Interface Sci. 572, 246–256.
Bernard, E., Lothenbach, B., Le Goff, F., Pochard, I., Dauzères, A., 2017. Effect of magnesium on calcium silicate hydrate (CSH). Cem. and concr. Res. 97, 61–72.
Brewitz, W., 1982. Ablauf und Ergebnisse der Eignungsuntersuchung der Schachtanlage Konrad für die Endlagerung radioaktiver Abfälle: Zusammenfassung. Gesellschaft für Strahlen-und Umweltforschung. Technical Report GSF-T 136, 131.
Bube, C., Metz, V., Bohnert, E., Garbev, K., Schild, D., Kienzler, B., 2013. Long-Term cement corrosion in chloride-rich solutions relevant to radioactive waste disposal in rock salt–Leaching experiments and thermodynamic simulations. Phys. Chem. Earth, Parts A/B/C 64, 87–94.
Carnall, W.T., 1992. A systematic analysis of the spectra of trivalent actinide chlorides in D 3 h site symmetry. J. Chem. Phys. 96, 8713–8726.
Colàs, E., Grivé, M., Rojo, I., Duro, L., 2013. The effect of gluconate and EDTA on thorium solubility under simulated cement porewater conditions. J. Solut. Chem. 42, 1680–1690.
Dario, M., Molera, M., Allard, B., 2004. Effect of Organic Ligands on the Sorption of Europium on TiO_2 and Cement at High pH. Swedish Nuclear Fuel and Waste Management Co., Stockholm, Sweden. Technical Report TR-04-04, SE-102 40.
DiBlasi, N.A., Tasi, A.G., Trumm, M., Schnurr, A., Gaona, X., Fellhauer, D., Dardenne, K., Rothe, J., Reed, D.T., Hixon, A.E., 2022. Pu (iii) and Cm (iii) in the presence of EDTA: aqueous speciation, redox behavior, and the impact of Ca (ii). RSC Adv. 12, 9478–9493.
Edelstein, N.M., Klenze, R., Fanghänel, T., Hubert, S., 2006. Optical properties of Cm (III) in crystals and solutions and their application to Cm (III) speciation. Coord. Chem. Rev. 250, 948–973.
Fanghänel, T., Kim, J.-I., 1998. Spectroscopic evaluation of thermodynamics of trivalent actinides in brines. J. Alloys Compd. 271, 728–737.
Garbev, K., Bornefeld, M., Beuchle, G., Stemmermann, P., 2008. Cell dimensions and composition of nanocrystalline calcium silicate hydrate solid solutions. Part 2: X-ray and thermogravimetry study. J. Am. Ceram. Soc. 91, 3015–3023.
Giffaut, E., Grivé, M., Blanc, P., Vieillard, P., Colàs, E., Gailhanou, H., Gaboreau, S., Marty, N., Made, B., Duro, L., 2014. Andra thermodynamic database for performance assessment: ThermoChimie. Appl. Geochem. 49, 225–236.
Grangeon, S., Claret, F., Linard, Y., Chiaberge, C., 2013. X-ray diffraction: a powerful tool to probe and understand the structure of nanocrystalline calcium silicate hydrates. Acta Crystallogr. B: Struct. Sci. Cry. Eng. Mat. 69, 465–473.
Guidone, R.E., 2023. Impact of Formate, Citrate and Gluconate on the Retention Behavior of Pu(III/IV), Cm(III) and Eu(III) by Cement Phases. Thesis. Karslruhe Institute for Technology (KIT).
Häusler, F., 2023. C-S-H Phase Formation and Solubility Behavior against the Background of the Use of Cement in Final Storage Concepts for Radioactive Waste. Thesis. Technische Universität Bergakademie Freiberg.
Häußler, V., Amayri, S., Beck, A., Platte, T., Stern, T.A., Vitova, T., Reich, T., 2018. Uptake of actinides by calcium silicate hydrate (C-S-H) phases. Appl. Geochem. 98, 426–434.
Holleman, A.F., 2019. Lehrbuch der anorganischen Chemie. Walter de Gruyter GmbH & Co KG, Berlin, 91 - 100.
Hummel, W., Anderegg, G., Puigdomènech, I., Rao, L., Tochiyama, O., 2005. The OECD/NEA TDB review of selected organic ligands. Radiochim. Acta 93, 719–725.
Keith-Roach, M.J., 2008. The speciation, stability, solubility and biodegradation of organic co-contaminant radionuclide complexes: a review. Sci. Total Environ. 396, 1–11.
Kimura, T., Choppin, G.R., 1994. Luminescence study on determination of the hydration number of Cm (III). J. Alloys Compd. 213, 313–317.
Lersow, M., Waggitt, P., 2020. Disposal of All Forms of Radioactive Waste and Residues, 1. Switzerland.
Li, K., Pang, X., 2014. Sorption of radionuclides by cement-based barrier materials. Cem. and concr. Res. 65, 52–57.
Lothenbach, B., Nonat, A., 2015. Calcium silicate hydrates: solid and liquid phase composition. Cem. and concr. Res. 78, 57–70.

Macé, N., Wieland, E., Dähn, R., Tits, J., Scheinost, A.C., 2013. EXAFS investigation on U (VI) immobilization in hardened cement paste: influence of experimental conditions on speciation. Radiochim. Acta 101, 379–389.
Mandaliev, P., Stumpf, T., Tits, J., Dähn, R., Walther, C., Wieland, E., 2011. Uptake of Eu (III) by 11 Å tobermorite and xonotlite: a TRLFS and EXAFS study. Geochim. Cosmochim. Acta, GCA 75, 2017–2029.
Maragkou, E., Pashalidis, I., 2021. Investigations on the interaction of EDTA with calcium silicate hydrate and its impact on the U (VI) sorption. Coat. 11, 1037.
Monshi, A., Foroughi, M.R., Monshi, M.R., 2012. Modified Scherrer equation to estimate more accurately nano-crystallite size using XRD. WJNSE 2, 154–160.
Myers, R.J., L'Hôpital, E., Provis, J.L., Lothenbach, B., 2015. Effect of temperature and aluminium on calcium (alumino) silicate hydrate chemistry under equilibrium conditions. Cem. and concr. Res. 68, 83–93.
Nonat, A., 2004. The structure and stoichiometry of C-S-H. Cem. and concr. Res. 34, 1521–1528.
Ochs, M., Dolder, F., Tachi, Y., 2022. Decrease of radionuclide sorption in hydrated cement systems by organic ligands: comparative evaluation using experimental data and thermodynamic calculations for ISA/EDTA-actinide-cement systems. Appl. Geochem. 136, 105161.
Ochs, M., Mallants, D., Wang, L., 2016. Radionuclide and Metal Sorption on Cement and Concrete, 29. Switzerland.
Osterhage, W., Frey, H., 2022. Organisation der nuklearen Entsorgung. In: Transformation radioaktiver Abfälle: Von der Zwischenlagerung über die Endlagerung bis zur Transmutation. Springer, pp. 141–147.
Parkhurst, D.L., Appelo, C., 2013. Description of input and examples for PHREEQC version 3—a computer program for speciation, batch-reaction, one-dimensional transport, and inverse geochemical calculations. US geo. survey tech.method. 6, 497.
Pointeau, I., Hainos, D., Coreau, N., Reiller, P., 2006. Effect of organics on selenite uptake by cementitious materials. Waste Manag. 26, 733–740.
Pointeau, I., Piriou, B., Fedoroff, M., Barthes, M.-G., Marmier, N., Fromage, F., 2001. Sorption mechanisms of Eu3+ on CSH phases of hydrated cements. J. Colloid Interface Sci. 236, 252–259.
Rübel, A.P., Müller-Lyda, I., Storck, R., 2004. Die Klassifizierung radioaktiver Abfälle hinsichtlich der Endlagerung. Gesellschaft für Anlagen- und Reaktorsicherheit (GRS) mbH. Technical Report GRS-203.
Schlegel, M.L., Pointeau, I., Coreau, N., Reiller, P., 2004. Mechanism of europium retention by calcium silicate hydrates: an EXAFS study. Environ. Sci. Technol. 38, 4423–4431.
Stumpf, T., Tits, J., Walther, C., Wieland, E., Fanghänel, T., 2004. Uptake of trivalent actinides (curium (III)) by hardened cement paste: a time-resolved laser fluorescence spectroscopy study. J. Colloid Interface Sci. 276, 118–124.
Szabo, P., Tasi, A., Gaona, X., Maier, A., Hedström, S., Altmaier, M., Geckeis, H., 2022. Uptake of selected organic ligands by hardened cement paste: studies on proxy ligands for the degradation of polyacrylonitrile and general considerations on the role of different functionalities in the uptake process. Frontiers. Nuclear. Eng. 1, 997398.
Tasi, A., Gaona, X., Fellhauer, D., Böttle, M., Rothe, J., Dardenne, K., Polly, R., Grivé, M., Colas, E., Bruno, J., 2018. Thermodynamic description of the plutonium–α–d–isosaccharinic acid system ii: formation of quaternary Ca (II)–Pu (IV)–OH–ISA complexes. Appl. Geochem. 98, 351–366.
Tasi, A., Gaona, X., Rabung, T., Fellhauer, D., Rothe, J., Dardenne, K., Lützenkirchen, J., Grivé, M., Colàs, E., Bruno, J., 2021. Plutonium retention in the isosaccharinate–cement system. Appl. Geochem. 126, 104862.
Taylor, H.F., 1986. Proposed structure for calcium silicate hydrate gel. J. Am. Ceram. Soc. 69, 464–467.
Tits, J., Stumpf, T., Rabung, T., Wieland, E., Fanghänel, T., 2003. Uptake of Cm (III) and Eu (III) by calcium silicate hydrates: a solution chemistry and time-resolved laser fluorescence spectroscopy study. Environ. Sci. Technol. 37, 3568–3573.
Tits, J., Wieland, E., 2018. Actinide Sorption by Cementitious Materials. PSI Bericht Nr. 18-02 Paul Scherer Institut, CH-5232 Villingen. PSI, Switzerland.
Tits, J., Wieland, E., Müller, C., Landesman, C., Bradbury, M., 2006. Strontium binding by calcium silicate hydrates. J. Colloid Interface Sci. 300, 78–87.
Wieland, E., 2014. Sorption Data Base for the Cementitious Near-Field of L/ILW and ILW Repositories for Provisional Safety Analyses for SGT-E2. PSI Bericht Nr. 14-08 Paul Scherer Institut, CH-5232 Villingen, PSI, Switzerland.
Xiong, Y., Kirkes, L., Westfall, T., 2017. Experimental determination of solubilities of di-calcium ethylenediaminetetraacetic acid hydrate [$Ca_2C_{10}H_{12}N_2O_8 \cdot 7H_2O$ (s)] in NaCl and $MgCl_2$ solutions to high ionic strengths and its Pitzer model: applications to geological disposal of nuclear waste and other low temperature environments. Chem. Geol. 454, 15–24.
Yan, Y., Yang, S.-Y., Miron, G.D., Collings, I.E., L'Hôpital, E., Skibsted, J., Winnefeld, F., Scrivener, K., Lothenbach, B., 2022. Effect of alkali hydroxide on calcium silicate hydrate (CSH). Cem. and concr. Res. 151, 106636.